Double photoionization of helium

Steven L. Carter and Hugh P. Kelly

Department of Physics, University of Virginia, Charlottesville, Virginia 22901

(Received 24 February 1981)

Many-body perturbation theory is applied to calculate double-electron photoionization for helium. While lowest-order results show reasonable agreement with experiment, it is found that certain higher-order correlation effects are significant. Techniques are presented for approximating these effects in a calculation which is first order in electron correlations.

I. INTRODUCTION

Many-body perturbation theory (MBPT) serves to provide a particularly sensitive calculational method for electron-electron correlation effects when applied to the multiple ionization process. Unlike the perturbation series associated with one-electron photoionization calculations, there is no single lowest-order term to describe the double excitation process. Indeed, previous MBPT work on neon,[1,2] argon,[2] and beryllium[3] has revealed the rather delicate interference among the various amplitudes representing two-electron excitation. While these calculations have been moderately successful, there still remain a number of unanswered questions pertaining to electron screening, choice of potential, and higher-order correlation effects. Further study along these lines can be applied to a relatively simple atomic system wherein careful analysis of higher-order MBPT terms is technically feasible. Findings can then be easily extended to the more complicated systems.

In this paper we present the results of a calculation for the double photoionization cross section $\sigma^{2+}(\omega)$ of helium in the energy range extending from threshold to 290 eV. We have applied the MBPT of Brueckner[4] and Goldstone[5] using techniques developed for application of this theory to atoms.[6] A brief review is presented in Sec. II. Section III contains a discussion of special computational techniques and numerical results for $\sigma^{2+}(\omega)$. A summary follows in Sec. IV.

II. THEORY

As in previous work,[2] a perturbation expansion is developed for the imaginary part of the frequency-dependent dipole polarizability[6] $\alpha(\omega)$ for use in the relation[7]

$$\sigma^{2+}(\omega) = (4\pi\omega/c)\,\mathrm{Im}\alpha(\omega), \tag{1}$$

where ω is the photon energy and c is the speed of light. Atomic units are employed throughout

except where noted otherwise.

Neglecting the spin-orbit interaction and other relativistic effects, the expansion of $\mathrm{Im}\alpha(\omega)$ is applied to an atom with atomic Hamiltonian

$$H = H_0 + H_c, \tag{2}$$

where

$$H_0 = \sum_{i=1}^{N} -\frac{\nabla_i^2}{2} - \frac{Z}{r_i} + V(r_i) \tag{3}$$

and

$$H_c = \sum_{i<j=1}^{N} v_{ij} - \sum_{i=1}^{N} V(r_i). \tag{4}$$

The term v_{ij} represents the Coulomb interaction between electron pairs, and the single-particle potential $V(r_i)$ is chosen to account for the average interaction of the ith electron with the other N-1 electrons.

In the dipole approximation, a perturbing electric field proportional to $\hat{z}\cos\omega t$ leads to an expression for $\mathrm{Im}\alpha(\omega)$ in terms of the electric dipole matrix element. For two-electron photoionization, the dipole-length matrix elements are given by

$$Z(pq \to k'k) = \left\langle \Psi_f \left| \sum_{i=1}^{N} z_i \right| \Psi_0 \right\rangle, \tag{5}$$

where Ψ_0 and Ψ_f are correlated many-particle ground and continuum states, respectively, with Ψ_f representing the excitation of an electron pair from ground-state orbitals p and q to excited-state orbitals k' and k. The dipole velocity-form matrix element is obtained by replacing the matrix element in Eq. (5) by

$$(E_0 - E_f)^{-1} \left\langle \Psi_f \left| \sum_{i=1}^{N} \frac{\partial}{\partial z_i} \right| \Psi_0 \right\rangle, \tag{6}$$

where E_0 and E_f are energy eigenvalues corresponding to Ψ_0 and Ψ_f.

In a zero-order approximation, the correlated state Ψ is the unperturbed state Φ obtained from

$$H_0 \Phi = E^{(0)} \Phi, \tag{7}$$

where Φ is represented in LS coupling as a linear

combination of determinants, each containing N different single-particle states ϕ_n which are solutions of

$$\left(\frac{-\nabla^2}{2}-\frac{Z}{r}+V(r)\right)\phi_n=\epsilon_n\phi_n .$$ (8)

The unperturbed energy $E^{(0)}$ of Eq. (7) is then

$$E^{(0)}=\sum_{i=1}^{N}\epsilon_i .$$ (9)

The excited-state, single-particle continuum orbitals are normalized in the k scale[8] according to

$$P_k(r)=rR_k(r)$$
$$=\sin[kr+(q/k)\ln 2kr-l\pi/2+\delta_l] ,$$ (10)

where $V(r)\to q/r$ as $r\to\infty$. With this choice of normalization, Eq. (1) becomes

$$\sigma^{2+}(\omega)=\frac{16\omega}{c}\int_0^{k_{max}}dk\frac{|Z(pq\to k'k)|^2}{k'} ,$$ (11)

where

$$k'=[2(\epsilon_p+\epsilon_q-\tfrac{1}{2}k^2+\omega)]^{1/2}$$

and

$$k_{max}=[2(\epsilon_p+\epsilon_q+\omega)]^{1/2} .$$

Individual terms in the perturbation expansion for $Z(pq\to k'k)$ involve single-particle states and may be represented by open diagrams of the form shown in Figs. 1, 2, and 3. The lowest-order double photoionization diagrams contain one dipole interaction and one interaction with the electron-correlation perturbation H_c of Eq. (4), as shown in Figs. 1(a)–1(c). The time ordering of the interactions proceeds graphically from bottom to top, with diagram 1(a) representing ground-state correlations (GSC) and diagrams 1(b) and 1(c)

(a)   (b)

(c)   (d)
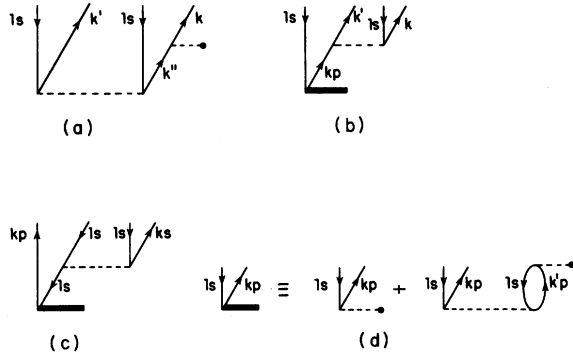
FIG. 1. Diagrams contributing to the matrix element $Z(pq\to k'k)$. Broken line ending with full circle indicates matrix element of z; other broken lines represent Coulomb interactions; heavy bar indicates correlated dipole matrix element. Exchange diagrams are also included.

(a)   (b)

(c)   (d)
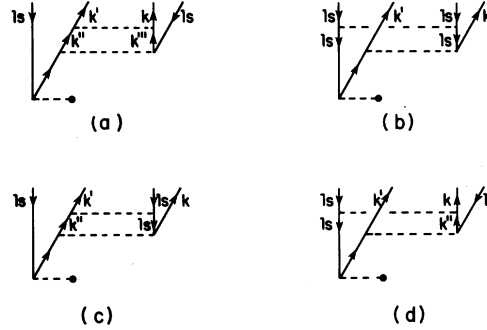
FIG. 2. Second-order FSC diagrams associated with ladder, hole-hole, and hole-particle interactions. Exchange diagrams are also included.

representing final-state correlations (FSC). Exchange diagrams are always understood to be included.

The general form of the unperturbed energy denominators occurring in GSC diagrams is

$$D=\sum_{i=1}^{N'}(\epsilon_{p_i}-\epsilon_{k_i}) ,$$ (12a)

and for FSC diagrams,

$$D=\sum_{i=1}^{N'}(\epsilon_{p_i}-\epsilon_{k_i})+\omega ,$$ (12b)

where ϵ_{p_i} and ϵ_{k_i} are single-particle energies for a hole-particle pair, and N' is the number of pairs excited. In Eq. (12b) the cases in which the denominator may vanish are treated according to

$$\lim_{\eta\to0}(D+i\eta)^{-1}=\mathcal{P}D^{-1}-i\pi\delta(D) ,$$ (13)

where $\mathcal{P}$ represents principal-value integration.

Important classes of exclusion-principle-violating (EPV) diagrams[6] arise from two sources. In one case interactions with the potential (included in H_c) may lead to EPV diagrams of the type shown in Figs. 1(c), 2(c), 2(d), 3(c), and 3(d). The Coulomb interaction portion of diagram 1(c),

(a)   (b)

(c)   (d)
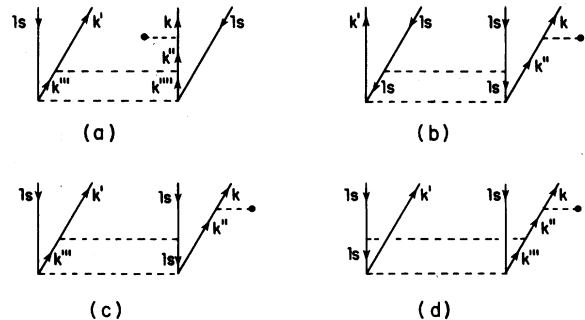
FIG. 3. Second-order GSC diagrams associated with ladder, hole-hole, and hole-particle interactions. Exchange diagrams are also included.

for example, is closely related to the monopole transition matrix element and can be associated with the electron shakeoff process.[9] Second-order EPV diagrams 2(c), 2(d), 3(c), and 3(d), containing hole-particle interactions, appear whenever the excited states k, k' of Fig. 2 and k', k'' of Fig. 3 are calculated in the commonly used Hartree-Fock (HF) V^{N-1} potential[6,10] (in which one core orbital is missing) and correct for the fact that these electrons now propagate in the absence of two core electrons. Such hole-particle interactions, therefore, partially account for electron screening effects. In the second case, EPV diagrams arise from the factorization of unlinked diagrams[6] in the expansion for $\alpha(\omega)$. The hole-hole interactions in EPV diagrams 2(b) and 3(b) are from this source and, along with the higher-order diagrams of this class, can be summed geometrically to produce shifts in the unperturbed energy denominators, corresponding to energy correlations. In Fig. 2(b), for example, the $1s$ hole-hole interaction shown is equivalent to the Slater[11] integral $F^0(1s1s)$ which in turn is just minus the $E^{(1)}$ correction to the unperturbed helium $1s^2$ ground-state energy $(2\epsilon_{1s})$.

In calculations of the lowest-order diagrams, higher-order energy correlation shifts can be included by appropriate insertion in the denominator expressions of Eq. (12). While this procedure correctly accounts for the hole-hole interactions to infinite order, there still remain both the particle-particle (ladder) and hole-particle interactions to consider. These diagrams are quite difficult to evaluate order by order but cannot be ignored for the following reason. Figure 4 illustrates the way in which these interactions first appear in correlation-energy diagrams[12] of third order when a V^{N-1} potential is used. It is known that diagrams 4(b) and 4(c) have the opposite algebraic sign from diagrams 4(d) and 4(e), but since each of the four diagrams has about the same absolute magnitude,[12] they tend to cancel among themselves. Yet each one of these can be individually large. Diagram 4(b), for example, contains the hole-hole interactions which, along with diagram 4(a), together

(a) (b) (c)

(d) (e)
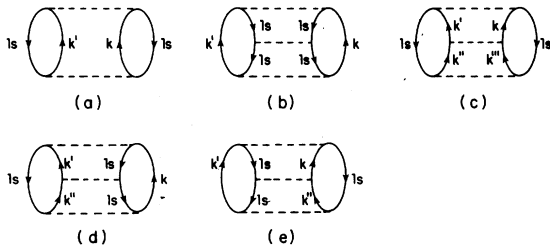
FIG. 4. Second- and third-order correlation energy diagrams. Exchange diagrams are also included.

form the first two terms in a geometric series that sums to produce the $E^{(1)}$ shift in the unperturbed denominator of diagram 4(a). For helium this $E^{(1)}$ correction is large and must be included, for example, in the appropriate FSC energy denominators of Eq. (12b) in order to reproduce the correct double ionization threshold. Such a procedure now makes it necessary to include both ladder and hole-particle interactions since omission of these terms will lead to a serious imbalance.

For double ionization diagrams, the ladder and hole-particle interactions occur both as corrections in the final state (shown explicitly in Fig. 2) and in the ground state (shown explicitly in Fig. 3). The corrections in the final state can be substantially reduced by simply calculating one set of continuum orbitals in a HF V^{N-1} potential (for electron k', say), and the remaining continuum orbitals in a HF V^{N-2} potential (for electron k). With this procedure, diagram 2(c) remains the same and corrects for the V^{N-1} potential used for electron k'. However, diagram 2(d) now vanishes since electron k is calculated as if both $1s$ core electrons were missing. Ladder diagram 2(a), which is always present, is then approximately canceled by the remaining diagram 2(c), and the cancellation continues order by order. The hole-hole interaction in diagram 2(b) is summed geometrically in the usual way with higher orders to yield the desired $E^{(1)}$ shift. Note that if electrons k and k' are both calculated in either V^{N-1} or V^{N-2} potentials, one cannot by this method effect cancellation of the higher-order diagrams. This would seem to suggest that screening in the final state may be intermediate between that obtained by using either V^{N-1} or V^{N-2} potentials for both excited states.

The ladder and hole-particle interactions of the ground-state correlations must be treated somewhat differently since the Fig. 3 particle lines labeled $k', k'', k''', $ and k'''' can all represent the same single set of excited states. If the set involves V^{N-1} orbitals, then the four Fig. 3 diagrams approximately cancel among themselves, as discussed earlier. The lowest-order GSC diagram of Fig. 1(a) should therefore be calculated with the unperturbed energy denominator of Eq. (12a) while omitting the Fig. 3 terms altogether. On the other hand, if the set involves the V^{N-2} orbitals, then diagrams 3(c) and 3(d) vanish. This leaves two diagrams, 3(a) and 3(b), of the same algebraic sign and of approximately the same magnitude. Diagram 3(b) and its higher orders can always be summed out exactly to yield an $E^{(1)}$-shifted denominator in diagram 1(a). The remaining diagram 3(a) and its higher orders can-

not be similarly summed. One can approximate their effects, however, by examining the correlation-energy diagrams of Fig. 4(c) containing the same ladder interactions. It is known from previous correlation-energy calculations[12] that, order by order, the ratio R of one diagram of a given class to the same class diagram of the previous order is approximately constant. One can thus determine R by explicitly calculating diagrams 4(a) and 4(c) and taking their ratio. Relative to diagram 1(a), the effects of ladder diagram 3(a) and all higher orders can then be approximated by the geometric factor $(1-R)^{-1}$ which multiplies diagram 1(a). Since R is generally negative (for ladder interactions), diagram 3(a) and its higher orders effectively reduce the lowest-order amplitude, as does the $E^{(1)}$ shift.

An additional small reduction can be expected from the l-changing[12] portions of Figs. 2(a) and 3(a). As opposed to the diagonal or ladder-type interactions, electrons k''' and k'''' of Figs. 3(a), for example, can have l values different from electrons k' and k''. Although not insignificant, such l-changing interactions are generally smaller than the corresponding ladder interactions. If desired, they can be included in a manner similar to that used for the ladder interactions.

III. CALCULATIONS AND RESULTS

The transition matrix elements $Z(pq \to k'k)$ of Eqs. (5) and (6) were calculated for the two partial-wave channels corresponding to $1s^2 \to kskp\,^1P$ and $1s^2 \to kpkd\,^1P$. Additional channels of the form $1s^2 \to k_l k_{l+1}\,^1P$ with $l>1$ are expected to be quite small and were therefore omitted. The radial $1s$ orbital for neutral helium was obtained from the Hartree-Fock (HF) code of C. F. Fischer.[13] Additional sets of excited bound and continuum orbitals were calculated in the HF frozen-core approximation using both V^{N-1} and V^{N-2} potentials (see Table I).

The $V^{N-1}kp$ potential was derived from the configuration $1skp\,^1P$. This choice ensures that correlation matrix elements of the form

$$\langle 1skp\,^1P\,|H_c|\,1sk'p\,^1P\rangle$$

vanish[10] so that the first-order FSC correction to

TABLE I. One-electron Hartree-Fock potentials.

State	$V(r)^a$
ks	$|1s\rangle\langle 1s|\,J_{1s}^0$
kp	$J_{1s}^0 + \frac{1}{3}K_{1s}^1$
kd	0

$^a J_a^\kappa|b\rangle \equiv \int_0^\infty dr'\,\phi_a(r')\phi_a(r')(r_<^\kappa/r_>^{\kappa+1})\phi_b(r);\ K_a^\kappa|b\rangle$
$\equiv \int_0^\infty dr'\,\phi_a(r')\phi_b(r')(r_<^\kappa/r_>^{\kappa+1})\phi_a(r).$

the one-electron transition matrix element

$$\langle 1skp\,^1P\,|z|\,1s^2\,^1S\rangle$$

also vanishes. This leaves only one first-order GSC correction as shown in Fig. 1(d). The excited kd orbitals were chosen to be pure hydrogenic V^{N-2} states, as were the ks states with the addition of a projection term[14] to ensure orthogonality with the HF $1s$ orbital. In effect, all s states (including the $1s$) were calculated from the same Hermitian potential,

$$J_{1s}^0 + (1 - |1s\rangle\langle 1s|)(-J_{1s}^0)(1 - |1s\rangle\langle 1s|),$$

which when applied to the $1s$ orbital reduces to J_{1s}^0, but when applied to an excited s state reduces to the form shown in Table I. All of the s states are therefore mutually orthogonal.

For each l value, eight bound excited states were explicitly calculated, with the contribution from the remainder approximated by the n^{-3} rule.[6] For sums over states, the continuum was approximated by 28 orbitals ranging from $k=0.1$ to $k=14.0$. Individual diagrams of Fig. 1 were evaluated radially in the usual manner by a sum over intermediate bound states and integral over the continuum. Only diagram 1(a) is difficult to evaluate by this technique because of the radial integrations in the k'' to k dipole matrix elements when both k'' and k represent continuum orbitals. An alternative method involves application of the differential-equation or effective-operator[15] approach described in detail in a previous work.[2] This method was used in the evaluation of both diagram 1(a) and the correlation-energy diagrams of Fig. 4.

The correlated matrix element $Z(pq \to k'k)$ is constructed from the sum of the diagrams of Fig. 1 using LS-coupled wave functions to determine the appropriate angular factors. Exchange diagrams are always understood to be included. Diagram 1(c), of course, appears only in the $1s^2 \to kskp$ channel. The final matrix element is numerically represented as a square matrix of 15 preselected continuum k values ranging from $k=0.1$ to $k=4.0$. The finer k mesh required for the integration in Eq. (11) is developed via a four-point Lagrange interpolation procedure which can be appropriately adjusted for each photon energy ω.

As discussed in Sec. II, the effects of the second- and higher-order FSC interactions of Fig. 2 are nearly canceled by using the V^{N-1} and V^{N-2} combination for electrons k' and k. However, one can explicitly examine the effects of the higher-order GSC interactions of Fig. 3 by calculating diagram 1(a) both with and without the appropriate corrections. Lowest-order dipole-length and velocity
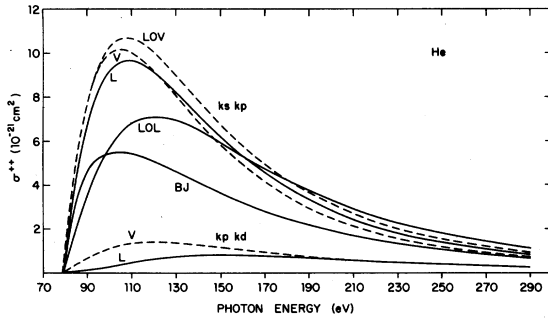
FIG. 5. Theoretical calculations of σ^{2+} for helium.
Curves labeled LOL (LOV) are lowest-order dipole-
length (dipole-velocity) results for the $kskp$ channel.
Curves labeled L (V) are length (velocity) results con-
taining higher-order corrections for both $kskp$ and
$kpkd$ channels. Curve labeled BJ is dipole-velocity
result from Byron and Joachain (Ref. 20).

cross sections for the channel $1s^2 \rightarrow kskp$ are shown
in Fig. 5 as calculated from the Fig. 1 diagrams,
having first omitted all corrections to diagram
1(a). Agreement between length (LOL) and velo-
city (LOV) curves is rather poor in the region
near maximum, with the velocity curve domin-
ating. This lack of agreement is not totally unex-
pected when one examines the individual diagrams
of Fig. 1. It is found that separate FSC and GSC
diagram totals, while individually large and of
nearly the same magnitude, are of opposite signs
and therefore interfere strongly, with the FSC
contribution being the larger of the two. The over-
all transition amplitude $Z(pq \rightarrow k'k)$ can thus be
sensitive to rather small corrections in the GSC
total.

For the $kskp$ channel, diagram 1(a) appears
twice, once with labels k, k', $k'' = kp$, ks, $k's$ and
once with labels k, k', $k'' = ks$, kp, $k'p$. For the
latter case, use of V^{N-1} kp states leads to near
cancellation among the second-order corrections
of Fig. 3. Diagram 1(a) therefore remains uncor-
rected for k, k', $k'' = ks$, kp, $k'p$. When k, k',
$k'' = kp$, ks, $k's$, however, use of V^{N-2} ks states
requires that diagrams 3(c) and 3(d) vanish. Dia-
gram 3(b) and its higher orders were then summed
geometrically with diagram 1(a) to yield the $E^{(1)}$
denominator shift. For helium, $E^{(1)} = -F^0(1s1s)$
$= -1.0258$, and since $\epsilon_{1s} = -0.91796$, the quantity
$2\epsilon_{1s} + E^{(1)} = -2.8617$ which is quite close to the ex-
perimental[16] $1s^2$ energy of -2.9034. The remain-
ing ladder diagram of Fig. 3(a) and its higher
orders were approximated as discussed in Sec.
II. By explicitly calculating the energy correla-
tion diagrams in Figs. 4(a) and 4(c), we deter-
mined the ratio R to be $0.005476/-0.02014$
$= -0.2718$, giving a multiplicative factor, $(1 - R)^{-1}$
$= 0.786$. Diagram 1(a) (as labeled k, k', $k'' = kp$,

ks, $k's$) was then recalculated using the $E^{(1)}$-
shifted denominator and the multiplicative factor
$(1 - R)^{-1}$. Figure 5 shows the resulting $kskp$ dip-
ole-length (L) and velocity (V) cross sections as
calculated with these modifications. Besides a
marked improvement in agreement between length
and velocity curves, one finds a general shifting
of the length-form oscillator strength toward the
lower energy region. As in a previous work,[2] the
length curve appears to be more sensitive to the
higher-order corrections.

A similar analysis was applied in the $kpkd$ chan-
nel. Of the two GSC diagrams of Fig. 1(a), the one
with labels k, k', $k'' = kp$, kd, $k'd$ requires mod-
ification due to the use of V^{N-2} kd orbitals. The
$E^{(1)}$ shift remains the same, while the factor
$(1 - R)^{-1}$ was determined to be 0.890. Modified
$kpkd$ length (L) and velocity (V) curves are shown
in Fig. 5. Although we found little improvement
over the uncorrected results, a careful analysis
shows that GSC diagram 1(a) with k, k', $k'' = kp$,
kd, $k'd$ is quite small compared with the one
labeled k, k', $k'' = kd$, kp, $k'p$. This second GSC
diagram is uncorrected in our approximation
scheme do to the use of V^{N-1} kp orbitals. However,
a small reduction in the magnitude of this diagram
was found to improve the length and velocity agree-
ment significantly, again with little change in the
velocity curve. Such a reduction can be attributed
to any number of higher-order effects but is most
probably due to omission of l-changing diagrams
of the type also represented by Figs. 2(a) and 3(a).
The overall smallness of the $kpkd$ cross section is
due, not so much to the smallness of individual
diagrams, but rather to the nearly complete can-
cellation between FSC and GSC diagram groups.
Length and velocity cross sections are therefore
extremely sensitive to small corrections in either
of these groups. This is in contrast to the $kskp$
diagram sums in which the FSC totals dominate.

Comparison with experiment and other theoreti-
cal calculations is shown in Fig. 6. Our result
(solid curve) for the σ^{2+}/σ^+ ratio is based on the
geometric mean of the length (L) and velocity (V)
curves of Fig. 5 including the contribution from
the $kpkd$ channel which is seen to be significant
at the higher photon energies. Matrix elements
for determining $\sigma^+(n = 1)$ were calculated using the
HF V^{N-1} $1skp$ ^1P continuum orbital set and corre-
lated as in Fig. 1(d). Data for $\sigma^+(n = 2)$ in the 80–
160-eV range were taken from the recent calcula-
tion by Chang.[17] Beyond 160 eV the $\sigma^+(n = 2)/\sigma^+(n$
$= 1)$ ratio was estimated to fall linearly to the val-
ue[18] 0.048 at 600 eV. Contributions from $\sigma^+(n > 2)$
were approximated[19] as an overall 2% of $\sigma^+(n = 1)$.

Curves labeled BJ and Br are from earlier
velocity-form calculations by Byron and Joachain[20]
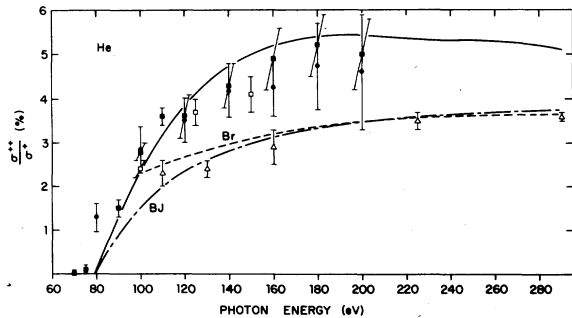
FIG. 6. The σ^{2+}/σ^+ ratio for helium. Curves are theoretical calculations. Solid curve, this work; broken curve, Brown (Ref. 21); chain curve, Byron and Joachain (Ref. 20); experimental data points are from Holland et al. (Ref. 23), full circles; Schmidt et al. (Ref. 23), open squares; Wight and Van der Wiel (Ref. 23), full squares; Carlson (Ref. 9), open triangles.

FIG. 7. Theoretical calculations of the total σ^{2+} for helium. Curves for the correlated length (L) and velocity (V) cross sections include contributions from both $kskp$ and $kpkd$ channels. Experimental data are from Bizau et al. (Ref. 25).

and by Brown,[21] respectively, which are both based on a fully correlated initial-state wave function but representing the final state as a symmetrized product of uncorrelated Coulomb wave functions, each seeing a charge of $Z = 2$. In contrast to this approach which neglects correlations in the final state, the MBPT technique predicts that ground- and final-state correlations are equally important, with FSC terms actually being the larger of the two. Further, the MBPT results seem valid for either dipole-length or dipole-velocity matrix elements, whereas the BJ length (not shown) and velocity curves[20] exhibit rather poor agreement. The BJ velocity-form cross section is shown explicitly in Fig. 5. Although the BJ curve and our correlated $kskp$ velocity curve are quite close in the high-energy region, there is a factor of 2 discrepancy in the threshold region. This difference is not so apparent in the Fig. 6 ratios because of different data[20] used for $\sigma^+(\omega)$.

A curious feature of our calculated ratio in Fig. 6 is the very shallow dip in the curve near 230 eV. An even larger dip occurs when σ^{2+} results are normalized to the experimental σ^+ data of Marr and West.[22] That structure of this type actually exists in the σ^{2+}/σ^+ ratio is uncertain, although a similar dip occurs, for example, when the BJ curve of Fig. 5 is normalized to the Marr and West data.[22]

In the region from threshold to 200 eV, our results are in relatively good agreement with recent experimental measurements.[23] Only the curve representing the geometric mean is shown in Fig. 6, but ratios based on the individual length and velocity results of Fig. 5 both lie within the error bars of most of the experimental data points. Beyond 290 eV our curve also appears to join rea-

sonably well with the asymptotic calculation by Amusia et al.,[24] whose curve begins at about 295 eV with the approximate value of 4.9%.
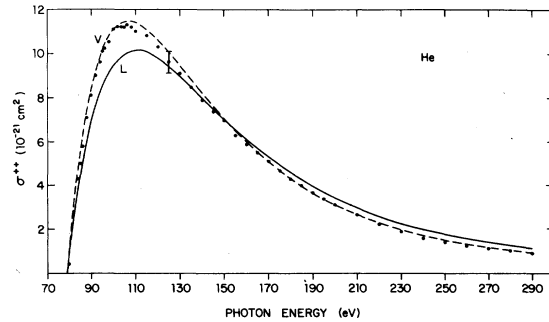
After this paper was submitted for publication we received from Dr. F. Wuilleumier the results of a very recent experimental measurement[25] of the absolute $\sigma^{2+}(\omega)$ for helium. These results are shown in Fig. 7 along with our calculated length and velocity totals taken from Fig. 5. Our velocity curve, in particular, shows excellent agreement with these data and may suggest that the velocity-form calculation is more accurate. This is consistent in general with our observation that velocity matrix elements are less sensitive to higher-order corrections.

IV. CONCLUSIONS

Application of many-body perturbation techniques has been found to provide an accurate description of double photoionization in helium. The use of combination V^{N-1} and V^{N-2} continuum orbitals has been shown to eliminate to a large degree electron-screening effects which appear in higher-order FSC diagrams that would otherwise be difficult to evaluate. Separate analysis of double ionization amplitudes arising from ground- and final-state correlations indicates that there is a delicate interference between the two correlation types. An appreciable cancellation occurs, in particular, for the $kpkd$ cross section. This cross section, although small, must be included for good agreement with experiment in the higher-energy region. Contributions from additional partial-wave channels of the form $k_l k_{l+1}$ are expected to be negligible.

Based on the results of this work, it is expected that use of these simple techniques for inclusion

of higher-order effects will apply equally well in more complicated systems. A reexamination of double photoionization in neon, for example, would be especially useful. A previous first-order MBPT calculation[2] which excluded these effects produced curves somewhat similar to the *kskp* length curve (LOL) of Fig. 5 in which the slope of the cross section is too shallow near threshold and in which the maximum is shifted toward the higher-energy region. Inclusion of the higher-order cor-

rections would presumably improve agreement with experiment.

[1]T. N. Chang, T. Ishihara, and R. T. Poe, Phys. Rev. Lett. **27**, 838 (1971); T. N. Chang and R. T. Poe, Phys. Rev. A **12**, 1432 (1975).

[2]S. L. Carter and H. P. Kelly, Phys. Rev. A **16**, 1525 (1977).

[3]P. Winkler, J. Phys. B **10**, L693 (1977).

[4]K. A. Brueckner, Phys. Rev. **97**, 1353 (1955); *The Many Body Problem* (Wiley, New York, 1959).

[5]J. Goldstone, Proc. R. Soc. (London) Ser. A **239**, 267 (1957).

[6]H. P. Kelly, Adv. Theor. Phys. **2**, 75 (1968).

[7]U. Fano and J. W. Cooper, Rev. Mod. Phys. **40**, 441 (1968).

[8]H. A. Bethe and E. E. Salpeter, *Quantum Mechanics of One- and Two-Electron Atoms* (Springer, Berlin, 1957).

[9]T. A. Carlson, Phys. Rev. **156**, 142 (1967).

[10]M. Ya. Amus'ya, N. A. Cherepkov, and L. V. Chernysheva, Zh. Eksp. Teor. Fiz. **60**, 160 (1971) [Sov. Phys—JETP **33**, 90 (1971)].

[11]J. C. Slater, *Quantum Theory of Atomic Structure* (McGraw-Hill, New York, 1960), Vol. I.

[12]H. P. Kelly, Phys. Rev. **131**, 684 (1963).

[13]C. F. Fischer, Comput. Phys. Commun. **4**, 107 (1972).

[14]L. M. Frantz, R. L. Mills, R. G. Newton, and A. M. Sessler, Phys. Rev. Lett. **1**, 340 (1958); B. A. Lippmann, M. H. Mittleman, and K. M. Watson, Phys. Rev. **116**, 920 (1959); R. T. Pu and E. S. Chang, *ibid.* **151**,

31 (1966); H. J. Silverstone and M. L. Yin, J. Chem. Phys. **49**, 2026 (1968); S. Huzinaga and C. Arnau, Phys. Rev. A **1**, 1285 (1970).

[15]R. M. Sternheimer, Phys. Rev. **115**, 1198 (1959).

[16]C. E. Moore, *Atomic Energy Levels*, U. S. Natl. Bur. Stand. Circ. No. 467 (U. S. GPO, Washington, D. C., 1949).

[17]T. N. Chang, J. Phys. B **13**, L551 (1980).

[18]V. L. Jacobs and P. G. Burke, J. Phys. B **5**, L67 (1972).

[19]F. Wuilleumier and M. Y. Adam, J. Phys. (Paris) Lett. **41**, L373 (1980).

[20]F. W. Byron, Jr., and C. J. Joachain, Phys. Rev. **164**, 1 (1967).

[21]R. L. Brown, Phys. Rev. A **1**, 586 (1970).

[22]G. V. Marr and J. B. West, At. Data Nucl. Data Tables **18**, 498 (1976).

[23]V. Schmidt, N. Sander, H. Kuntzemuller, P. Dhez, F. Wuilleumier, and E. Källne, Phys. Rev. A **13**, 1748 (1976); G. R. Wight and M. J. Van der Wiel, J. Phys. B **9**, 1319 (1967); D. M. P. Holland, K. Codling, J. B. West, and G. V. Marr, *ibid.* **12**, 2465 (1979).

[24]M. Ya Amusia, E. G. Drukarev. V. G. Gorshkov, and M. P. Krazachkov, J. Phys. B **8**, 1248 (1975).

[25]J. M. Bizau, F. Wuilleumier, D. Ederer, P. Dhez, S. Krummacher, and V. Schmidt, J. Phys. (Paris) (in press).